ACS OMEGA

http://pubs.acs.org/journal/acsodf

Article

Synthesis, Self-Aggregation, Surface Characteristics, Electrochemical Property, Micelle Size, and Antimicrobial Activity of a Halogen-Free Picoline-Based Surface-Active Ionic Liquid

Nidhi N. Patel, Saurabh S. Soni, Niraj Patel, Kiran Patel, Vaibhav K. Patel, Deep Sharma, and Sanjay H. Panjabi*

Cite This: *ACS Omega* 2022, 7, 28974−28984

Read Online

ACCESS | Metrics & More | Article Recommendations | Supporting Information

ABSTRACT: We present a new approach toward the design of a halogen-free picoline-based surface-active ionic liquid (SAIL) (1-octyl-4-methyl pyridinium dodecyl sulfate) [$C_8\gamma$Pic]DS consisting of long dodecyl sulfate (DS) as an anion. The surface properties, micellization behavior, and antimicrobial activity in an aqueous solution were investigated using tensiometry, conductometry, and ultraviolet (UV) spectroscopy. Incorporating the DS group in SAIL leads to lower critical micellar concentration (CMC) and enhanced adsorption at the air/water interface of the functionalized ionic liquid compared to the C_8-alkyl chain-substituted pyridine ionic liquids. The antimicrobial activity was evaluated against a representative Gram-negative and Gram-positive bacteria panel. Antibacterial activities increased with the alkyl chain length, C_8 being the homologous most effective antimicrobial agent. The micelle size of [$C_8\gamma$Pic]DS was determined by the dynamic light-scattering (DLS) study. Cyclic voltammetry (CV) measurements have been employed to evaluate the interaction between the SAIL micelle and working electrode, diffusion coefficient, and micelle size of the SAIL solution. The diffusion coefficient explored the correlation of surface properties and the antimicrobial activity of [$C_8\gamma$Pic]DS. This halogen-free SAIL is the future of wetting agents and emulsion studies in agriculture due to its small micelle size and surface characteristics.

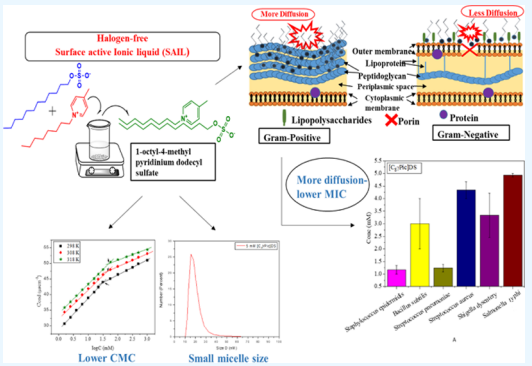

1. INTRODUCTION

As a new class of surfactants, ionic liquid-based surfactants have recently gained considerable interest. It has been shown that ionic liquids containing long alkyl chains are similar to traditional surfactants forming aggregates in water, which have evident amphiphilic properties and were regarded as new surfactants known as surface-active ionic liquids (SAILs).[1−3] Because of their structural characteristics, SAIL based on imidazolium is a class where the head and counterion replacement can be widely varied.[4,5] At present, the number of SAIL in the last decade increased due to the emerging need for chemicals in different fields. However, some critical concerns, such as the life cycle, reactivity, stability, and biodegradability of SAILs, have been studied.[6] However, most of the SAIL narratives in the document are narrowly focused on halogen-free SAILs. Thus, in the last few years, several greener amphiphiles based on structures have emerged, pointing out alkyl carboxylate,[7,8] amino acid,[9] and alkyl sulfate-based[10] SAILs free from halogen. The high tunability of SAIL opens up a wide range of applications, for example, in micellar catalysis, analytical chemistry, and electrochemical science.[10,11] During the last decade, alternative solvents have been introduced in diver's electrochemical applications, i.e., ionic liquid (ILs). Wang et al. reported SAILs with enhanced surface properties compared to conventional surfactants and revealed their applications.[12] SAILs can also exhibit significant biological activity against bacteria and fungi.[13] In the reaction mechanism, separation or extraction process, and product yield, the molecular state of such ionic liquids in an aqueous system is expected to play a vital role. Pandey and group explored the application of ILs in biphasic separation.[14] In addition to the application, Zeng and group discovered the S-doped porous g-C_3N_4, which was fabricated using an ionic liquid.[15] For example, suppose aggregates of ILs are present in the system, they can interfere in a reaction as there may be undesired solubilization within the associates or may thermodynamically affect the response.

Despite the above-listed features, few studies deal with the colloidal chemical aspects of ILs based on amphiphilic methyl pyridinium. On the other hand, some authors have noted that changing the functional group of the ILs changes the

Received: April 27, 2022
Accepted: August 4, 2022
Published: August 15, 2022

antimicrobial activity.[16,17] For example, a significant decrease in antimicrobial activity was reported for imidazolium SAILs containing amide side chains than alkyl-substituted derivatives.[9] Morrissey et al. reported a notable reduction in the antimicrobial activity containing the ether or polyether side chains of imidazolium ILs, compared with the alkyl-substituted derivatives.[18] In contrast, Garcia et al., introducing a cationic mixture of SAIL and *N*-lauroyl sarcosinate, observed a broad spectrum of antimicrobial activity against bacteria.[19] Ana et al. synthesized a new class of SAILs from chloroquine (CQ) and fatty acids, which shows superior in vitro antimicrobial activity compared to the parent drug.[20] Another group of Feder-Kubis discovered terpene-based ionic liquids, which behaved as selective agents in antifungal therapy.[21]

The potential of these ILs is an interest in increasing the fundamental data in such devices as rechargeable batteries, electrochromic devices, etc.[22] Cyclic voltammetry (CV) is widely regarded as one of the most important electrochemical methods due to its excellent potency. In addition, CV data give vital information about the kinetics of electron transfer of heterogeneous reactions, thermodynamics of redox and oxidation processes, and the process of adsorption or a coupled chemical reaction. Many studies were conducted to screen the electrochemical window (EW)s of ILs. This is the initial stage in determining the appropriateness of the investigated ILs for the desired electrochemical applications. Lee and group discovered that the optimized electrochemical anodization treatment could significantly improve the descaling efficiency at least 50 times faster in an ionic liquid environment.[23] Water content is one of the most important elements influencing O'mahony et al. utilized the CV method to examine the EW.[24] McEwen and group found that the EWs for $[BF_4]^-$-based ILs are approximately 3.5 and 4.0 V for bis(trifluoromethylsulfonyl)-imide [TFSI]-based ILs.[25] The surfactant's electrochemical behavior was investigated to evaluate the micellar size. The diffusion coefficient of the surfactants can be assessed using the Randles−Sevcik equation with the peak current (i_p) of each solution.[22] Asit et al. determined the diffusion coefficient and CMC of the sodium dodecyl sulfate (SDS), TX-100, and Tween-80 using the Randles−Sevcik and the Stokes−Einstein relation equation.[26] The size and shape of micelles are usually determined by a light-scattering method. However, Tsuyoshi et al. revealed the solution properties of micelles composed of fluorocarbon surfactants in which they determined the diffusion coefficient with the hydrodynamic micelle radius.[27]

In addition, ILs based on pyridinium cations are promising as they are surface-active and result in a successful biodegradable soft matter.[28] As a result, a perfect understanding of the aggregation behavior of long alkyl chain amphiphilic SAILs is an attractive study field in colloid and interface science from basic and practical perspectives. Therefore, the present study reports the synthesis, aggregation behavior, micelle size, and thermodynamic and antimicrobial activity that correlate with the diffusion coefficient and the surface parameters of picoline-based SAIL. Furthermore, the present work is expected to be used to study the properties of emulsifiers and wetting agents.

2. METHODS AND MATERIALS

2.1. Materials. 4-Methylpyridine (99%), 1-chlorooctane (>99.9%), and sodium dodecyl sulfate (SDS) were used as received. The solutions of the SAIL were prepared in distilled water for measurement.

2.2. Synthesis of SAIL.

- In a round-bottom flask, 15.00 g (0.161 mol) of 4-methylpyridine was taken, and 23.93 g (0.161 mol) of 1-chlorooctane was added dropwise and heated at 353.15 K for 48 h. The liquid product was cooled, and ethyl acetate was added with thorough mixing. The excess ethyl acetate was decanted, and the same process was repeated 4 times. After final washing, the traces of ethyl acetate (if present) were removed by heating under a vacuum for 12 h. 1-Octyl-4-methyl pyridinium chloride $[C_8\gamma Pic]Cl$ was obtained with a worked-out yield of 85.00%. The corresponding ^1H NMR spectra are shown in Figure S1.
- A solution of $[C_8\gamma Pic]Cl$ (35 mmol) was mixed with sodium dodecyl sulfate (35 mmol) in CH_2Cl_2, and sodium chloride salt was removed by filtration. The two phases were separated with a separating funnel. The organic phase containing SAIL was washed several times with water 10 × 10 × 10 cm^3 until it was free of chloride (tested by $AgNO_3$). After removing the solvent in a rotatory evaporator, the product $[C_8\gamma Pic]DS$ was obtained as a white liquid (70.82%) (Scheme 1).

Scheme 1. Chemical Structure of 1-Octyl-4-methyl Pyridinium Dodecyl Sulfate ($C_{26}H_{49}NO_4S$)[a]

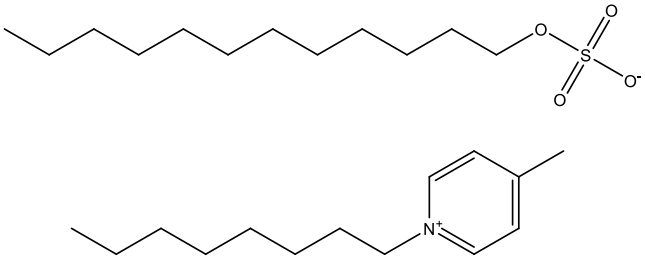

1-octyl-4-methylpyridinium dodecyl sulphate

[a]The NMR chemical shifts and assigned protons atoms are: ^1H NMR (400 MHz, D_2O, δ−ppm): 8.68 (q, 2H, CH), 7.80 (q, 2H, CH), 4.90 (m, 2H, CH2), 3.90 (t, 2H, CH_2), 2.51 (s, 3H, CH_3), 1.52 (m, 2H, CH_2), 1.15 (m, 30H, CH_2), 0.75 (t, 6H, CH_3) (Figure S2).

3. EXPERIMENTAL SECTION

3.1. Thermogravimetric Analysis (TGA). A Mettler Toledo thermal analyzer under a nitrogen environment was used to determine the decomposition temperature of the SAIL.

3.2. Conductometry. A digital conductivity meter was used to determine the electrical conductivity of SAIL in the water system at 298−318 K temperature (Systronics India Ltd., India), with the conductivity cell having a cell constant of 1 cm^{-1}. Aqueous solutions of KCl (0.01−1 M) were used to verify the cell constant θ, and the specific conductivity of the aqueous solutions was calculated. The uncertainty in the measurements was ±0.3%.

3.3. Surface Tension. The surface-active parameters for the SAIL in the aqueous system at 25 °C were determined using a tensiometer (Krüss K12 tensiometer, Biolin Scientific, China) with an uncertainty of ±0.1 mN m^{-1}.

3.4. DLS. Dynamic light-scattering (DLS) measurements were performed at 25 °C for an aqueous SAIL solution using a ζ-sizer (Nano-S90, Malvern Instruments) to measure the hydrodynamic particle size. The wavelengths of the laser and the scattering angle were 633 nm and 90°, respectively.

https://doi.org/10.1021/acsomega.2c02612
ACS Omega 2022, 7, 28974−28984

3.5. Electrochemical Measurements. Cyclic voltammetry (CV) was performed using an electrochemical workstation (CHI660 E, CHI) at −1.2 to 1.0 V at a 5 mV/S scan rate. In CV, three-electrode systems were used. A platinum wire was used as a counter, glassy carbon was used as a working electrode, and a saturated calomel electrode (SCE) was used as a reference electrode.

3.6. UV Spectroscopy. The ultraviolet (UV) absorption spectra of the sample were recorded using a UV−vis spectrophotometer (Shimadzu UV 1800, Japan). The spectra were recorded in the 180−400 nm wavelength range at 25 °C. Pyrene was used as a probe, and concentration was kept constant (1×10^{-6} mol dm^{-3}) in all experiments.

3.7. Antimicrobial Activity. The antimicrobial activity of the synthesized SAIL was determined based on the minimum inhibitory concentration (MIC) values against two Gram-negative, *Shigella dysentery* (MTCC 1457) and *Salmonella typhi* (MTCC 98), and four Gram-positive, *Staphylococcus epidermidis* (MTCC 3382), *Bacillus subtilis* (MTCC 411), *Streptococcus pneumoniae* (MTCC 655), and *Streptococcus aureus* (MTCC 96), bacterial strains. The detailed procedure for this activity is given in Supporting Section 1.1.

4. RESULT AND DISCUSSION

4.1. Thermal Analysis. Figure 1 depicts a typical thermogram of [$C_8\gamma$Pic]DS. Thermogravimetric analysis was performed in the temperature range of 25−550 °C, at a heating rate of 10 °C per minute. The data from the analysis indicates that the decomposition of the SAIL occurs in three steps as shown in the figure. In the TGA and derivative thermogravimetry (DTG) thermogram, the first weight loss around 35−145 °C corresponds to the loss of a water molecule; this loss of weight is more likely linked to the thermal breakdown/hydrolysis of the SAIL (which causes the formation/vaporization of secondary byproducts).[30] The second decomposition observed in the range of 193−348 °C is attributed to the decomposition of the hydrocarbon chain (DS^-), and the last decomposition indicates the degradation of the cationic moiety ($C_8\gamma Pic^+$).

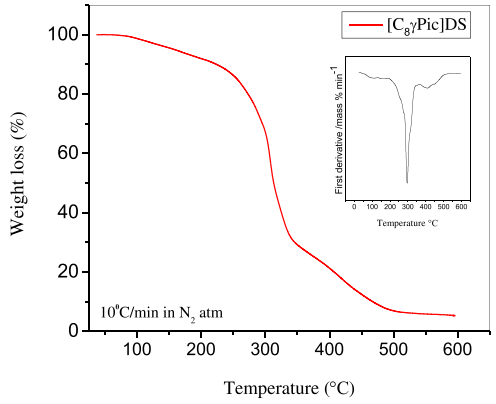

Figure 1. TGA curve of [$C_8\gamma$Pic]DS.

4.2. Conductance Measurements. Electrical conductivity measurement was applied to study the micellar aggregate formation of SAIL. Figure 2 reveals the change in the electrical conductivity (k) depending on the concentration of [$C_8\gamma$Pic]DS in a temperature range of 25−45 °C. It is evident that the progressive increase in the SAIL concentration results in two pieces that fit into two straight lines with a significant variation in the slope, which is caused by micelle formation, and the intersection of the two consecutive lines is ascribed to critical micellar concentration (CMC), which is shown in Table 2. From Table 2, it is seen that the reduction of CMC occurs when the anion of [$C_8\gamma$Pic]Cl will change from Cl to DS. [$C_8\gamma$Pic]Cl has a CMC of 175 mM, while in the case of [$C_8\gamma$Pic]DS, it is 1.5 mM, which is 100 times lower. As the establishment of the CMC will depend upon the molecule's hydrophobic nature, it was visually differentiated that [$C_8\gamma$Pic]DS had 12 extra carbon chains rather than [$C_8\gamma$Pic]Cl. With increasing temperature, the CMC values of [$C_8\gamma$Pic]DS increase slightly, which is similar to the case for the reported SAILs, [C_4mim][$C_{12}H_{25}SO_3$][31] and [C_{12}eim]Br,[32] and conventional ionic surfactants. The ratio of the slopes of postmicellar to premicellar plots of specific conductivity vs concentration plots can estimate the degree of counterion dissociation (β). As shown in Table 2, values of the β increase as temperature increases due to the high mobility of micelle formation (Table 1).

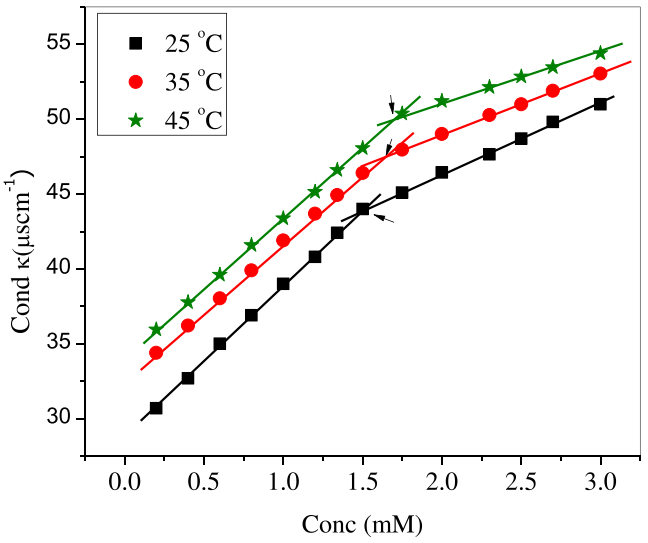

Figure 2. Plots of electrical conductivity vs concentration of aqueous solutions of SAIL at different temperatures.

Table 1. Description of Chemicals and Solvents Used

chemical name	source	CAS no.	purity (%)
4-methylpyridine	Sigma-Aldrich	108-89-4	99
1-chlorooctane	Sigma-Aldrich	111-85-3	99.0
sodium dodecyl sulfate	Sigma-Aldrich	151-21-3	≥99.0
dichloromethane	Sigma-Aldrich	75-09-2	≥99.8

4.2.1. Standard Free Energy of Micellization (ΔG_m°). The determination of thermodynamic parameters of micellization standard free energy change (ΔG_m°) plays an essential role in developing micelles, which is discussed as follows

$$\Delta G_m^\circ = (1 + \beta)RT \ln X_{cmc} \quad (1)$$

where X_{CMC} is the mole fraction, R is the gas constant, and β is the degree of counterion dissociation discussed earlier. Calculated thermodynamical parameters for [$C_8\gamma$Pic]DS at different temperatures are reported in Table 2. The [$C_8\gamma$Pic]DS moiety reduces electrostatic repulsions between the head and tail groups, preferring micellization and resulting in a more negative free energy transfer. The values of ΔG_m° become more negative as temperature increases in SAIL, showing that

https://doi.org/10.1021/acsomega.2c02612
ACS Omega 2022, 7, 28974−28984

Table 2. Value of CMC with Standard Error, Temperature (T), Degree of Counterion Dissociation (β), Gibbs Free Energy of Micellization (ΔG_m°), Standard Enthalpy of Micellization (ΔH_m°), and Standard Entropy Change (ΔS_m°) for SAILs at Different Temperatures[a]

SAIL	temp (°C)	COND CMC (mM)	β	ΔG_m° (kJ/mol)	ΔH_m° (kJ/mol)	$T\Delta S_m^\circ$ (kJ/mol)
[$C_8\gamma$Pic] DS	25	1.50	0.44	−34.08	−7.82	26.26
	35	1.61	0.45	−35.39	−8.41	26.99
	45	1.7	0.47	−36.46	−9.02	27.44
[$C_8\gamma$Pic] Cl[35]	25	175	0.46	−20.80	−1.59	64.60
[C_8Py] Cl[35]	25	180	0.43	−20.40	−1.49	63.40
[bmim] DS[36]	25	2.04	0.61	−24.68	−7.14	17.58

[a]Standard uncertainties are ΔG_m° = ±0.02 (kJ mol^{-1}), ΔH_m° = ±0.01 (kJ mol^{-1}), and $T\Delta S_m^\circ$ = ±0.02 (kJ mol^{-1}).

micellization is spontaneous. The presence of DS enhances the spontaneous aggregate formation via the transfer of the hydrophobic tail from the bulk solution to the micelle phase, as shown in Table 2.

4.2.2. Standard Enthalpy Change (ΔH_m°). The enthalpy of micellization was determined using the following equation

$$\Delta H_m^\circ = -RT^2(1+\beta)\left(\frac{\mathrm{d}\ln X_{cmc}}{\mathrm{d}T}\right) \quad (2)$$

where $[\mathrm{d}(\ln X_{CMC})/\mathrm{d}T]$ denotes the slope of the straight line of $\ln X_{CMC}$ vs temperatures. According to Table 2, the standard enthalpy of micellization value is negative. As the hydrogen bonds between water molecules weaken, less energy is required to break up the water cluster, which holds the structure's hydrocarbon chain over the whole temperature range.

4.2.3. Standard Entropy Change (ΔS_m°). The entropy of micellization was determined using eq 3

$$\Delta S_m^\circ = \frac{(\Delta H_m^\circ - \Delta G_m^\circ)}{T} \quad (3)$$

and the obtained values increased as the temperature increased, as tabulated in Table 2. Therefore, the micellization process is governed by the entropy gain associated with [$C_8\gamma$Pic]DS. It stands for the fact that the negative value of ΔG_m° is mainly due to ΔS_m°, which implies the method of micellization of [$C_8\gamma$Pic]DS.

4.2.4. Standard Free Energy of Adsorption (ΔG_{ads}°). The standard free energy of adsorption (ΔG_{ads}°) at the air/water interface was calculated using eq (4)[33]

$$\Delta G_{ads}^\circ = \Delta G_m^\circ - (\Pi_{CMC}/\Gamma_{max}) \quad (4)$$

where ΔG_m° is the standard free energy of micellization, and Π_{CMC} and Γ_{max} are listed in Table 3. DS is hydrophobic in nature and easy to form a micelle. The introduction of the DS as an anion into the SAIL causes an increase in the hydrophobicity nature of the molecule, as evidenced by the increase in the value of ΔG_{ads}°. Therefore, the ΔG_{ads}° value is superior to the ΔG_m° value.

4.2.5. Free Energy at the Air/Water Interface (ΔG_{min}^s). The value of ΔG_{min}^s is a transition of free energy of the bulk phase of a system at the air/water interface determined by the following equation.[34]

$$\Delta G_{min}^s = A_{min}\cdot\gamma_{CMC}\cdot N_A \quad (5)$$

The value of ΔG_{min}^s is defined as a free energy shift accompanied by a transition from the bulk phase of the solution to the surface component of the solution. The lowest free energy [$C_8\gamma$Pic]DS = 4.73 KJ/mol is more thermodynamically stable, which is measured to evaluate the synergism compared to [$C_8\gamma$Pic]Cl = 18.85 kJ/mol and [C_8Py]Cl = 21.76 kJ/mol (Table 3).

4.3. Surface Parameters. The surface tension was measured to evaluate the CMC and the surface activity of the SAIL in aqueous solutions. The solutions' surface tension (γ) was plotted against log C, as shown in Figure 3. The surface

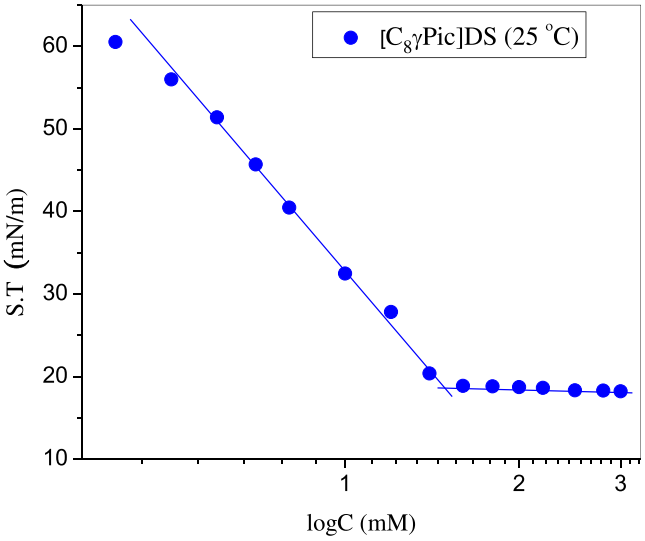

Figure 3. Surface tension as a function of log C of [$C_8\gamma$Pic]DS at 25 °C.

Table 3. CMC, Surface Excess Parameter (Γ_{max}), Minimum Surface Area Per Molecule (A_{min}), Surface Pressure at CMC (π_{CMC}), Adsorption Efficiency (pC_{20}), Surface Tension at CMC (γ_{CMC}), Standard Free Energy of Adsorption (ΔG_{ads}°), and Free Energy at the Air/Water Interface (ΔG_{min}^s) for [$C_8\gamma$Pic]DS at 25 °C[a]

SAIL	CMC ST (mM)	CMC UV (mM)	$T_{max}\times10^{10}$ (mol/cm^2)	A_{min} (Å)^2	π_{CAC}	pC_{20}	γ_{CMC}	ΔG_{ads}°(kJ/mol)	ΔG_{min}^s (kJ/mol)
[$C_8\gamma$Pic]DS	1.48 ± 0.3	1.50 ± 0.2	4.52	36.73	53.40	3.23	18.59	−45.85	4.11
[$C_8\gamma$Pic]Cl[35]	175.00		1.65	101.00	40.70	2.20	31.00	−45.46	18.85
[BMPy]LS[40]	1.53 ± 0.10		4.91	34.00	35.70		36.50		
[C_8Py]Cl[35]	181.00		1.70	98.10	34.60	1.60	36.84	−40.75	21.76
[bmim]DS[36]	2.09	2.02	1.75	95.00	37.50			−46.12	
[C_8APyr]LS[19]	1.0 ± 0.1		2.0	82.00	44.30	4.10	27.70		
SDS[37]	8.21		3.11	53.00	32.29		39.68	−39.53	12.76

[a]Standard uncertainties are ΔG_{ads}°= ±0.01 (kJ mol^{-1}) and ΔG_{min}^s = ±0.03 (kJ mol^{-1}).

https://doi.org/10.1021/acsomega.2c02612
ACS Omega 2022, 7, 28974−28984

tension dropped rapidly as the concentration was increased before subsequently stabilizing. The surface parameters such as surface excess concentration (Γ_{max}), minimum surface area per molecule at the interface (A_{min}), surface tension at CMC (γ_{CMC}), the effectiveness of the adsorption efficiency (pC_{20}), and surface pressure at CMC (π_{CMC}) of the SAIL are provided in Table 3. The CMC value for [$C_8\gamma$Pic]DS is discovered by the break-in γ-log C curve, and γ_{CMC} is observed at the breakpoint, which is listed in Table 3. Therefore, the present study had a better result in the form of CMC compared with the data reported for SDS,[37] [C_4mim][$C_{12}SO_4$],[38] [$C_8\gamma$Pic]Cl,[35] and *N*-octylpyridinuim bromide [C_8Py]Br,[39] which have the same hydrophobic chain length.

Sastry and co-authors discovered that the increase in hydrophobicity of the SAIL decreases the CMC, which was observed for [$C_8\gamma$Pic]DS. The results (Table 3) evidently show that [$C_8\gamma$Pic]DS has relatively lower CMC and γ_{CMC} than [$C_8\gamma$Pic]Cl, [C_8Py]Br, and SDS, which reveals that [$C_8\gamma$Pic]DS display more excellent surface activity than ionic surfactants and imidazolium-, pyridinium-, or pyrrolium-based SAILs.[35] The difference in the surface tension of the SAILs due to the formation of micelles results because of the following two reasons: (1) the electrostatic and hydrophobic interaction at the air−water interface and (2) picoline has a bulky counterion, which makes the hydration process weaker, and counterions reduce the electrostatic repulsion between head groups. During the formation of micelles, it serves a similar role to the second hydrophobic chain (i.e., dodecyl on the counterion ring), resulting in the lower CMC and γ_{CMC} of [$C_8\gamma$Pic]DS. In addition, Jiao et al. showed that *N*-butyl-*N*-methylpyrrolidinium dodecyl sulfate ([C_4MP] [$C_{12}SO_4$]) could form micelles in an aqueous solution, and its CMC was 2.7 mmol/L, which is higher than that of [$C_8\gamma$Pic]DS.[10] Interestingly, the CMC value of [$C_8\gamma$Pic]DS is about 100-fold lower than [$C_8\gamma$Pic]Cl and less than a quarter of that for SDS (CMC = 8.2 mM).[35,38]

4.3.1. Maximum Surface Excess Concentration (Γ_{max}). The maximum surface excess concentration (Γ_{max}) at the air−water interface can be obtained from the slope value of ($d\gamma$/d ln C) using the Gibbs adsorption isotherm

$$\Gamma_{max} = -\frac{1}{nRT}\left(\frac{\partial\gamma}{\partial \ln C}\right) \quad (6)$$

where R is the molar gas constant (8.314 J mol^{-1} K^{-1}) and T is the absolute temperature. The number of ionic species present in the solution produced by the dissociation of SAIL molecules is denoted by n. The value of n = 2 for the SAIL, [$C_8\gamma$Pic]DS, contains a picoline ring with one positive charge and a counterion, i.e., dodecyl sulfate with one negative charge on it. The adsorption of [$C_8\gamma$Pic]DS at the air/solution interface is enhanced by the electrostatic repulsion between the cationic head group and the anion of [$C_8\gamma$Pic]DS, which, in turn, increases the maximum surface excess concentration, resulting in a higher value of the Γ_{max} (4.52 mol cm^{-2}) compared to [$C_8\gamma$Pic]Cl (1.65 mol cm^{-2}), as presented in Table 3. The property of adsorption in the bulk solution or on the interface layer of the SAIL molecule opens the door for various applications.[41] This reveals that aggregates' concentration is high at the surface and they have high surface activity compared to halogen-based SAILs, which give good antimicrobial activity.

4.3.2. Area Occupied by a Single Molecule (A_{min}). The values of the minimum area per molecule (A_{min}), i.e., the area occupied by a single surfactant that reflects the surface arrangement of SAIL at the air−liquid interface, have been obtained using eq (7)

$$A_{min} = \frac{1}{N_A\,\Gamma_{max}} \quad (7)$$

where N_A is Avogadro's number (6.022 × 10^{23} mol^{-1}). The calculated value of the A_{min} (41.5 A^2) is presented in Table 3. These data indicate that the values of Γ_{max} and A_{min} vary with the molecular structure, as replacing the Cl anion with DS allows the SAIL molecules to be more tightly packed at the air−liquid interface.

4.3.3. Surface Pressure at the CMC (π_{CMC}). The values of surface tension of the solvent (γ_0) and that of the SAIL solution at the CMC (γ_{CMC}) have been used to evaluate the surface pressure at the CMC (π_{CMC}), as shown in eq (8)

$$\Pi_{cmc} = \gamma_0 - \gamma_{cmc} \quad (8)$$

As the hydrophobic chain length increases, the SAIL becomes more effective in reducing surface tension, as shown by γ_{CMC} (Table 3). π_{CMC}, on the other hand, increases when the hydrophobicity of SAIL increases, indicating that the SAIL molecule is ordered asymmetrically in the lattice crystal, resulting in a more significant reduction in the micellar surface area.

4.3.4. Adsorption Efficiency (pC_{20}). The adsorption efficiency (pC_{20}) of the SAIL at the interface was evaluated by employing eq (9)

$$pC_{20} = \log\frac{1}{C_{20}} \quad (9)$$

where pC_{20} is defined as the negative logarithm of the concentration of the SAIL required to reduce the surface tension of the pure solvent by 20 mN/m; the values of the efficiency of the SAILs are shown in Table 3. Using adsorption efficiency values, you may compare SAIL adsorption effectiveness at the air/water interfaces. A higher pC_{20} value decreases surface tension more effectively. For example, [$C_8\gamma$Pic]DS has higher adsorption effectiveness at the interface than [$C_8\gamma$Pic]Cl because of the hydrophobic chain's elongation and the anion's size.

4.4. UV Spectroscopy. The [$C_8\gamma$Pic]DS absorbance behavior in the UV−visible region (180−300 nm) was examined in our spectrophotometric investigation. Pyrene is used as a UV probe in our studies. Figure 4 represents the magnification of the recorded spectra in the wavelength range of 180−300 nm. Two pyrene peaks are due to the ring structure, and pyrene's characteristic absorption peaks are at 223.46 and 258 nm, as shown in Figure 4. The one at 223.46 nm shows the most absorbance and is selected for different studies.

For wavelengths in this range, a typical absorption vs concentration figure indicates that up to a particular SAIL concentration, absorbance varies linearly with the concentration according to Beer−Lambert's law.

In general, a typical plot of absorbance vs concentration at a constant wavelength, i.e., 223.46 nm of [$C_8\gamma$Pic]DS, is shown in Figure 5, and the observed CMC of [$C_8\gamma$Pic]DS is presented in Table 3. Sudden absorption jumps (Figure 4) are caused by developed micelles, which live in a nonpolar environment.

The mechanism of SAIL's micellization to the pyrene interaction is based on two possible factors: (1) Naturally, pyrene is driven to settle in the micelle's nonpolar interior, which decreases the hydrophobic repulsion forces between water and

https://doi.org/10.1021/acsomega.2c02612
ACS Omega 2022, 7, 28974−28984

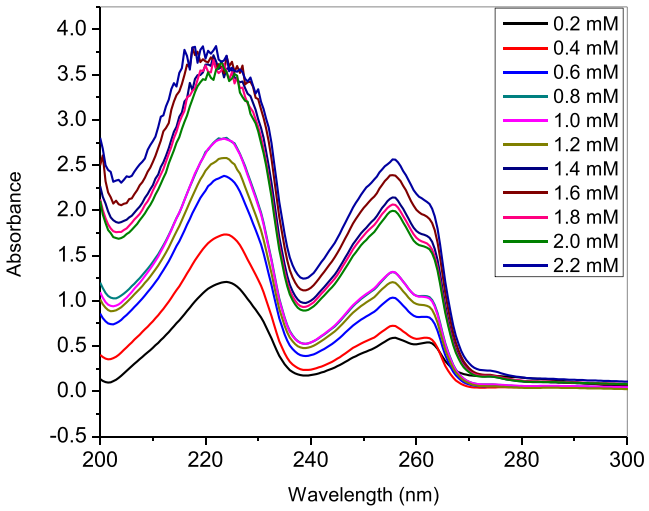

Figure 4. Absorbance spectra of [$C_8\gamma$Pic]DS at different concentrations.

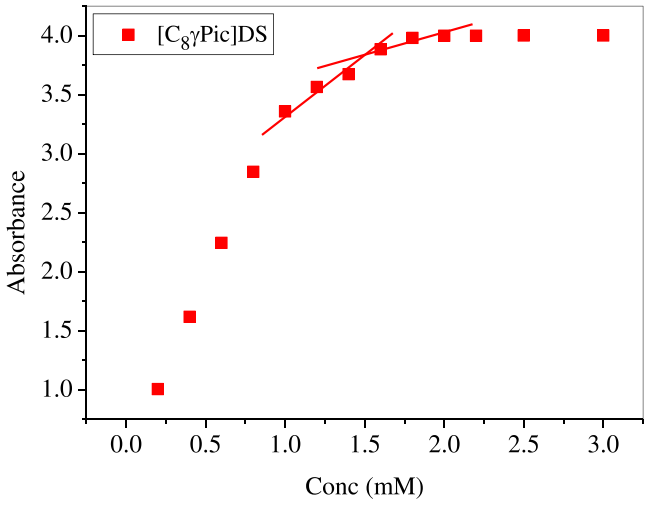

Figure 5. Plot of absorbance vs the changing concentrations of [$C_8\gamma$Pic]DS at a fixed wavelength of 223.46 nm.

pyrene and (2) there is no hydrophilic pyrene functionality that may draw pyrene to remain on the interface.[42] Nevertheless, it is clear that in this work, the CMC acquired by [$C_8\gamma$Pic]DS through spectroscopic methods is in good agreement with the value reported by conductometry and tensiometry.

4.5. DLS Study. DLS measurements were used to investigate the hydrodynamic radius of the SAIL at 298 K. In general, the distribution of size during the aqueous mass phase depends largely on the conformational modification of the molecular system, regardless of the volumetric profile's quantitative nature.[43] The number size distribution of [$C_8\gamma$Pic]DS above the CMC concentration is shown in Figure 6. Since [$C_8\gamma$Pic]DS behaved similarly at all concentrations, we have chosen a 5 mM solution for further study. C_{12}MeIm-LS aggregates with a hydrodynamic diameter (D_h) of ∼35 nm consistent with elongated micelles were detected, whereas, for C_{14}MeIm-LS, the presence of aggregates with a $D_h \geq 200$ nm was observed. Amide-functionalized SAIL-LS mixtures (C_8AMeIm-LS) homologues had a D_h of 22 nm, indicating micelle formation.[19] During analysis of a [$C_8\gamma$Pic]DS aqueous solution, using Stokes−Einstein relation eq (10), the diffusion coefficient

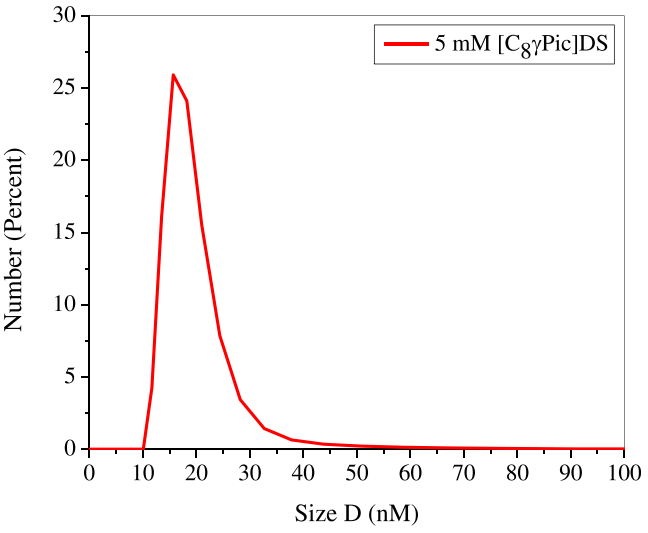

Figure 6. Size distribution curve of [$C_8\gamma$Pic]DS.

value for [$C_8\gamma$Pic]DS is 3.03×10^{-7} cm^2/s, and a single peak is observed with maximum intensities in the range of 10−30 nm.

$$r = k_B T / 6\pi\eta_o D \quad (10)$$

where k_B is denoted as the Boltzmann constant and ηo is denoted as the solvent's viscosity. DLS results showed a single distribution of the hydrodynamic radius, R_h ∼7.9 nm. It seems that the presence of a dodecyl sulfate (DS) group as an anion and a C_8 carbon chain at the $\gamma(\gamma)$ position to picoline promotes the aggregation of the micelle and smaller size compared to the nonfunctionalized SAIL. Notably, there is a rough correspondence with CV data.

4.6. Cyclic Voltammetry (CV). The cathodic potential value of the [$C_8\gamma$Pic]DS solution decreases due to electrostatic repulsion between SAIL micelles and OH^- shown in Figure 7.

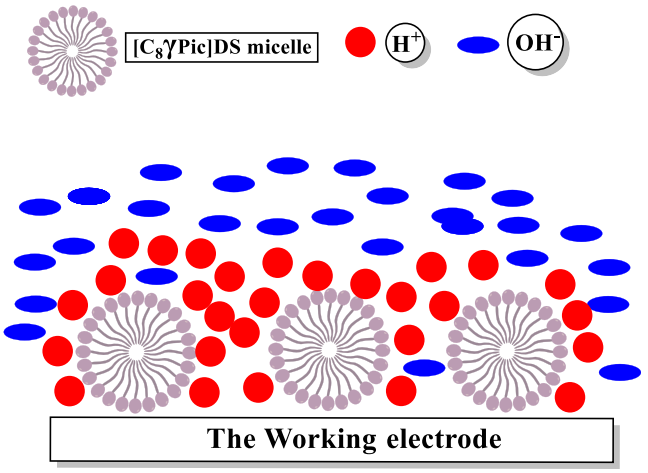

Figure 7. Schematic illustration of the mechanism of [$C_8\gamma$Pic]DS micelle solutions near the electrode.

Anodic peak size decreases when the adsorption process is taken by [$C_8\gamma$Pic]DS micelles near the working electrode, taking up the space of OH^-. A consequence of this interaction is the enrichment of H^+ ions around the surface of [$C_8\gamma$Pic]DS micelles due to the attraction between anionic and cationic ions. Enrichment with H^+ ions leads to a higher anodic current. Figure 8 shows the cyclic voltammograms of 5 mM [$C_8\gamma$Pic]DS in an

https://doi.org/10.1021/acsomega.2c02612
ACS Omega 2022, 7, 28974−28984

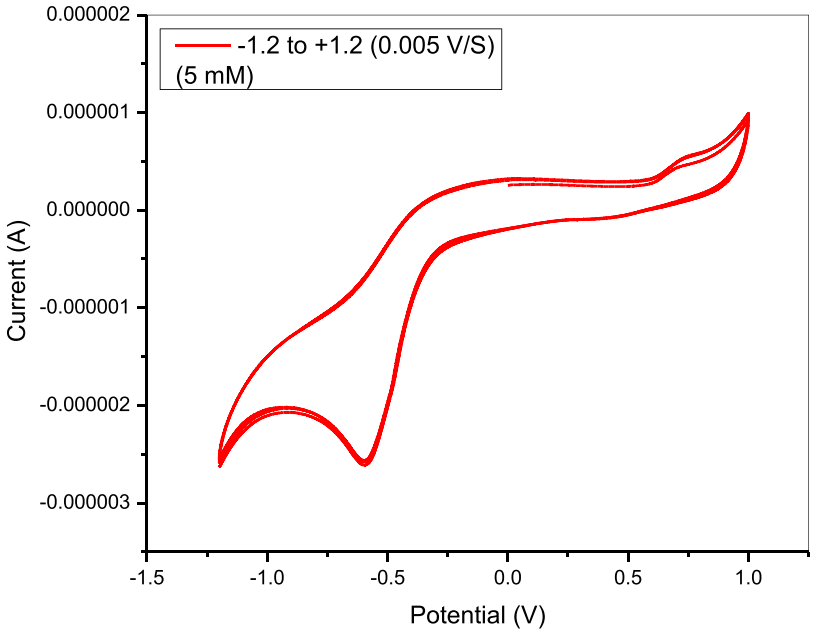

Figure 8. Cyclic voltammogram of the SAIL.

aqueous solution for various scan rates. The SAIL solution has the cathodic potential, which appears from −0.60 to −0.66 V, and the anodic potential appears from +0.08 to +0.12 V.

In cyclic voltammetry (CV), the peak i_p (μA) for a redox-active system is given by eq 11

$$i_p = \frac{0.447\, F^{3/2} A\, n^{3/2} D^{1/2} C v^{1/2}}{R^{1/2}\, T^{1/2}} \quad (11)$$

where F = Faraday constant, A = area of the electrode (cm^2), n = number of electrons involved in oxidation or reduction, D = diffusion coefficient of the electroactive species ($cm^2\ s^{-1}$), C = concentration of SAILs (M), ν = sweep rate ($V\ s^{-1}$), R = gas constant, and T = absolute temperature.

The potential was measured in a 5 mM solution of [$C_8\gamma$Pic]DS at a scan rate of 0.005 V s^{-1}. Therefore, eq 11 is rewritten as eq 12. The solution species oxidized or reduced at 303 K to get linear diffusion.

$$i_{pc} = 2.687 \times 10^5\, n^{3/2} A D^{1/2} C v^{1/2} \quad (12)$$

where A is the electrode area, n is the number of electrons involved in oxidation or reduction, D is the diffusion coefficient, C is the SAIL concentration, and v is the scan rate.

The diffusion coefficient was calculated from the slope of i_{pc} vs $v^{1/2}$, as shown in Figure 9. From the slope, the diffusion coefficient value for [$C_8\gamma$Pic]DS is 2.88×10^{-7} cm^2/s. Asakawa and group investigated the properties of the solution of micelles composed of fluorocarbon surfactants and ferro-cetyltrimethylammonium bromide (FcTAB) systems. The diffusion coefficient and the hydrodynamic radius of FcTAB in water were 5.9 $\times 10^{-6} cm^2/s$ and 4.1 Å, respectively. The diffusion coefficient significantly reduced with the increase in the salt concentration, implying an increase in micellar size and a change in the micelle form.[27] The hydrodynamic radius of [$C_8\gamma$Pic]DS obtained from the Stokes−Einstein relation (eq 10) was 8.33 nm. The value of the hydrodynamic radius and the diffusion coefficient were obtained from the CV data compared with DLS data.

4.7. Antimicrobial Activity. This study evaluated the antibacterial property of a picoline-based SAIL with an eight-carbon chain by measuring the minimum inhibitory concentration (MIC) values first and then comparing to those of other SAILs (Table 4). Compared to the decisive, broad-spectrum antibacterial action of short-chained ILs has poor biological activity. A series of microbial inhibition studies were performed on imidazolium ILs with varying chain lengths and anions.[2] Compared with other ILs, the imidazole-based SAIL with an eight-carbon chain compound 1-alkyl-3-methylimidazolium chloride, [OMIM]Cl, showed better activity than the butyl-[BMIM]Cl- and hexyl-[HMIM]Cl-substituted compounds. Their preferential adsorption at the bacterial cell wall disrupts the bacterial membrane due to the optimal hydrophilic/lipophilic balance.[44] There were also some changes in antibacterial activity between Gram-positive and Gram-negative bacteria. Gram-negative bacteria were shown to be similar or somewhat more resistant to the SAIL than Gram-positive bacteria. This might be attributed to the difference in

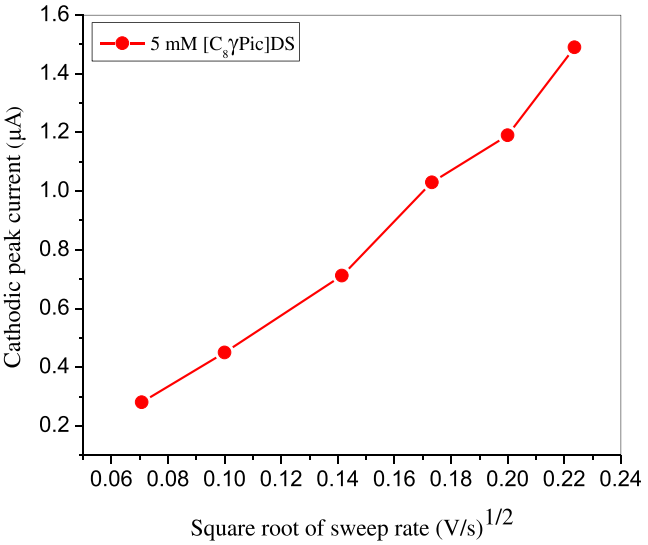

Figure 9. Plot of cathodic peak current vs square root of the sweep rate of 5 mM [$C_8\gamma$Pic]DS.

https://doi.org/10.1021/acsomega.2c02612
ACS Omega 2022, 7, 28974−28984

Table 4. Minimum Inhibitory Concentration (MIC) Values Represent Mean (n = 3) + Standard Error of [$C_8\gamma$Pic]DS against the Selected Gram-Positive (*S. epidermidis*, *B. subtilis*, *S. pneumoniae*, *S. aureus*) and Gram-Negative (*S. dysentery*, *S. typhi*) Bacterial Strains

	MIC (mM)			MIC (μM)
microorganism	[$C_8\gamma$Pic]DS	[CMPy]DS[29]	[CMPy]DBS[29]	C_{12}EPyrLS/C_{12}EMeIm-LS[19]
		Gram-Positive		
S. epidermidis	1.17 ± 0.06	4.83 ± 0.16	2.33 ± 0.16	31/8
B. subtilis	2.27 ± 0.07	1.80 ± 0.00	2.00 ± 0.00	31/16
S. pneumoniae	1.40 ± 0.11	0.90 ± 0.05	1.80 ± 0.05	
S. aureus	4.33 ± 0.16	5.33 ± 0.16	2.33 ± 0.16	31/16
		Gram-Negative		
S. dysentery	3.40 ± 0.11			
S. typhi	4.83 ± 0.16			

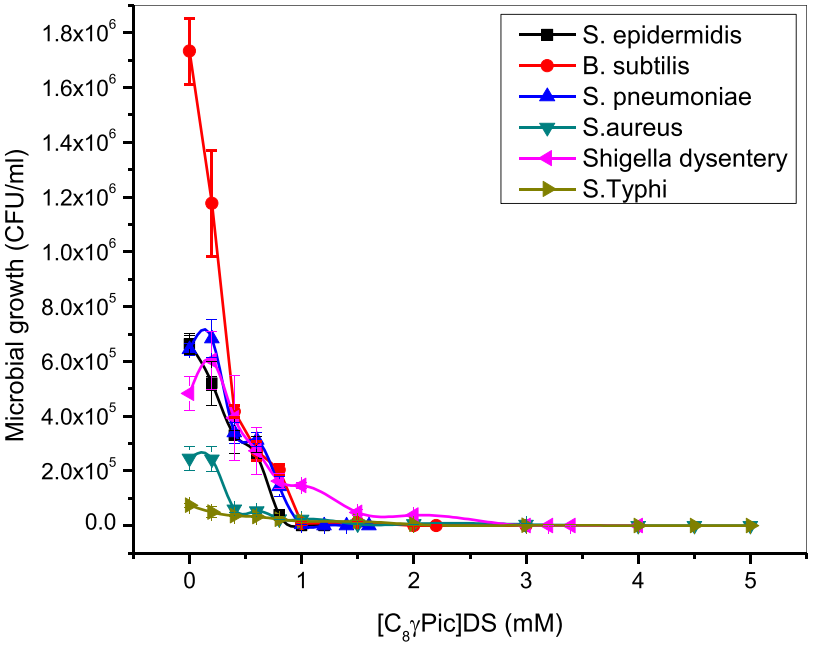

Figure 10. Growth curve of four gram-positive bacteria (*S. epidermidis*, *B. subtilis*, *S. pneumoniae*, *S. aureus*) and two gram-negative (*S. dysentery*, *S. typhi*) bacterial strains in the presence of different concentrations (0.1−5 mM) of [$C_8\gamma$Pic]DS values represent mean of CFU/mL (n = 3) ± standard error.

membranes and cell walls between different types and strains of bacteria. There is an additional lipopolysaccharide membrane presenting an additional barrier to Gram-negative bacteria. This barrier contributes to Gram-negative bacteria's high tolerance to [$C_8\gamma$Pic]DS. In addition, the bactericidal activity from cell viability curves has been determined by the colony forming unit (CFU) (Figure 10), in line with Carson et al.'s findings, which evaluate the antibiofilm activity of 1-alkyl-3-methylimidazolium chlorides to test the general applicability of ionic liquids as a biofilm. Gram-negative bacteria *Escherichia coli* had MIC = 722 μM and Gram-positive bacteria *S. epidermidis* had MIC = 361 μM for [C_8mim]Cl.[45] As a result, it can be observed (Table 4 and Figure 10) that [$C_8\gamma$Pic]DS had a greater efficacy against Gram-positive than Gram-negative bacteria. The antimicrobial activity of amide-functionalized ILs was evaluated against a panel of representative Gram-negative and Gram-positive bacteria and fungi.[9] In addition, without the functional group attached to the cation, halogen-free SAIL [$C_8\gamma$Pic]DS has better activity than the 3-alkoxy methyl-1-methylimidazolium salts of hexafluorophosphates, tetrafluoroborates, and chlorides.[46]

Diffusion is a function of the fluid, which includes the size of the penetrant and diffusing molecule, nature of the solvent, concentration, and solubility of the molecules. Moreover, the chances of [$C_8\gamma$Pic]DS reaching the microorganism's surface by diffusion are high, as the small area of molecules diffuses more rapidly. This phenomenon has been proved by the maximum value of surface excess concentration (Γ_{max} = 4.52 mol/cm^2) and the minimum surface area occupied by the single SAIL molecule at the air/liquid interface (A_{min} = 41.50 (Å)^2). Here, the diffusion coefficient was determined using the DLS and CV techniques with values of 3.03 × 10^{-7} and 2.88 × 10^{-7} cm^2/s, respectively. It is a simple relation among the Γ_{max}, A_{min}, and diffusion coefficient. (1) As the area occupied by each molecule decreases (A_{min}), it directly affects the surface of the liquid, which increases Γ_{max} and (2) the layer of the surface occupied by small molecules of the SAIL enhances the property of diffusion in the antimicrobial activity. The correlation of these three parameters results in a smaller molecular area and more surface excess concentration, which diffuses rapidly with the small value of the diffusion coefficient.

https://doi.org/10.1021/acsomega.2c02612
ACS Omega 2022, 7, 28974−28984

In addition, it can be said that a smaller A_{min} and a higher diffusion coefficient impacted the antimicrobial activity with a small amount of the SAIL concentration used to achieve the MIC value. Thus, the data presented here for the antimicrobial activity are essential to understanding the interaction between cell surface structures and existing wetting agents in the agriculture field.

5. CONCLUSIONS

This study uses picoline, octyl-chloride, and dodecyl sulfate as raw materials to synthesize a halogen-free alkyl sulfate-based SAIL (1-octyl-4-methyl pyridinium dodecyl sulfate) [$C_8\gamma$Pic]-DS, and the structure was confirmed by ^{1}H NMR spectroscopy. To investigate their adsorption at the air/liquid interface, thermodynamic parameters, and aggregation in aqueous solutions, several techniques were employed, namely, conductivity, surface tension, and UV spectroscopy. The observed study of this research is as follows:

(I) [$C_8\gamma$Pic]DS (1.60 mM) exhibited a 100-fold smaller CMC and interfacial and bulk properties in terms of γ_{CMC}, pC_{20}, A_{min}, etc., than their parent analogue, [$C_8\gamma$Pic]Cl (175 mM), and other conventional SAILs [Etmim]-[$C_{12}H_{25}SO_3$] (3.32 mM)[47] and C_8Pyr-LS (2.0 mM).[19] Micelle formations of SAIL were spontaneous and entropy-driven.

(II) The improved colloidal and surface behavior of the SAIL is due to the increased hydrophobicity of the SAIL caused by replacing a Cl anion with a DS hydrophobic counterion.

(III) The growing development of green technology demands new, biodegradable materials in which picoline-based SAILs significantly impact the microbes. Furthermore, SAILs exhibited different levels of sensitivity to Gram-positive and Gram-negative bacteria. Therefore, it can be observed that [$C_8\gamma$Pic]DS had a greater efficacy against Gram-positive than Gram-negative bacteria and acted as a broad-spectrum antimicrobial agent.

(IV) Here, DLS and cyclic voltammetry measurements revealed that the colloidal solutions of [$C_8\gamma$Pic]DS predominantly formed micelles having the hydrodynamic radii (R_h) ∼7.9 and ∼8.33 nm, respectively. The voltammetric analysis suggests that this reduction process occurs by the subsequent formation of an oxide phase on the electrode surface. The decreased diffusion coefficient value reflects the impact of the DS group on the SAIL as it helped decrease the micelle size and the CMC.

The lower CMC and smaller micelle size of [$C_8\gamma$Pic]DS enhance the understanding of aggregates in colloids and surface sciences. In addition, having the lower surface tension and surface parameters is expected to build the foundation for their properties in suitable applications like a wetting agent in agriculture, drug delivery, and nanomaterial fields.

ASSOCIATED CONTENT

Supporting Information

The Supporting Information is available free of charge at https://pubs.acs.org/doi/10.1021/acsomega.2c02612.

^{1}HNMR of [$C_8\gamma$Pic]Cl (Figure S1), ^{1}HNMR of [$C_8\gamma$Pic]-DS (Figure S2), and detailed procedure of antimicrobial activity (Section 1.1) (PDF)

AUTHOR INFORMATION

Corresponding Author

Sanjay H. Panjabi − *Department of Chemical Sciences, P. D. Patel Institute of Applied Sciences, CHARUSAT University, Changa, Gujarat 388421, India;* orcid.org/0000-0002-6653-7252; Phone: +91 9428435205; Email: sanjaypanjabi_27@yahoo.co.in

Authors

Nidhi N. Patel − *Department of Chemical Sciences, P. D. Patel Institute of Applied Sciences, CHARUSAT University, Changa, Gujarat 388421, India*

Saurabh S. Soni − *Department of Chemistry, Sardar Patel University, Anand, Gujarat 388120, India;* orcid.org/0000-0002-7584-4916

Niraj Patel − *Organic Chemistry Department, Institute of Science and Technology for Advanced Research (ISTAR), CVM University, Anand, Gujarat 388120, India*

Kiran Patel − *Director, Grow Leaf Biotech Private Limited, Anand, Gujarat 388120, India*

Vaibhav K. Patel − *Department of Chemical Sciences, P. D. Patel Institute of Applied Sciences, CHARUSAT University, Changa, Gujarat 388421, India*

Deep Sharma − *Department of Chemical Sciences, P. D. Patel Institute of Applied Sciences, CHARUSAT University, Changa, Gujarat 388421, India*

Complete contact information is available at: https://pubs.acs.org/10.1021/acsomega.2c02612

Notes

The authors declare no competing financial interest.

ACKNOWLEDGMENTS

The authors are grateful to Charotar University of Science and Technology (Charusat University) for providing research facilities to carry out research work. In addition, N.P. and D.S. acknowledge the Government of Gujarat for giving the "SHODH" Scholarship.

REFERENCES

(1) Jiao, J.; Han, B.; Lin, M.; Cheng, N.; Yu, L.; Liu, M. Salt-Free Catanionic Surface Active Ionic Liquids 1-Alkyl-3-Methylimidazolium Alkylsulfate: Aggregation Behavior in Aqueous Solution. *J. Colloid Interface Sci.* **2013**, *412*, 24−30.

(2) Wasserscheid, P.; Van Hal, R.; Bösmann, A. 1-n-Butyl-3-Methylimidazolium ([Bmim]) Octylsulfate - An Even "greener" Ionic Liquid. *Green Chem.* **2002**, *4*, 400−404.

(3) El Seoud, O. A.; Pires, P. A. R.; Abdel-Moghny, T.; Bastos, E. L. Synthesis and Micellar Properties of Surface-Active Ionic Liquids: 1-Alkyl-3-Methylimidazolium Chlorides. *J. Colloid Interface Sci.* **2007**, *313*, 296−304.

(4) Singh, O.; Singla, P.; Aswal, V. K.; Mahajan, R. K. Polymers Impact of Aromatic Counter-Ions Charge Delocalization on the Micellization Behavior of Surface-Active Ionic Liquids. *Langmuir* **2019**, *35*, 14586−14595.

(5) Ma, H.; Ke, H.; Wang, T.; Xiao, J.; Du, N.; Yu, L. Self-assembly of imidazolium-based surface active ionic liquids in aqueous solution: The role of different substituent group on aromatic counterions. *J. Mol. Liq.* **2017**, *240*, 556−563.

(6) Cho, C.-W.; Pham, T. P. T.; Jeon, Y. C.; Vijayaraghavan, K.; Choe, W. S.; Yun, Y.-S. Toxicity of Imidazolium Salt with Anion Bromide to a Phytoplankton Selenastrum Capricornutum: Effect of Alkyl-Chain Length. *Chemosphere* **2007**, *69*, 1003−1007.

(7) Lin, J. C. Y.; Huang, C. J.; Lee, Y. T.; Lee, K. M.; Lin, I. J. B. Carboxylic Acid Functionalized Imidazolium Salts: Sequential

Formation of Ionic, Zwitterionic, Acid-Zwitterionic and Lithium Salt-Zwitterionic Liquid Crystals. *J. Mater. Chem.* **2011**, *21*, 8110−8121.
(8) Cheng, N.; Yu, L.; Wang, T.; Sheng, X.; Bi, Y.; Gong, Y.; Yu, L. Self-Aggregation of New Alkylcarboxylate-Based Anionic Surface Active Ionic Liquids: Experimental and Theoretical Investigations. *J. Phys. Chem. B* **2014**, *118*, 2758−2768.
(9) Garcia, M. T.; Ribosa, I.; Perez, L.; Manresa, A.; Comelles, F. Self-Assembly and Antimicrobial Activity of Long-Chain Amide-Functionalized Ionic Liquids in Aqueous Solution. *Colloids Surf., B* **2014**, *123*, 318−325.
(10) Jiao, J.; Dong, B.; Zhang, H.; Zhao, Y.; Wang, X.; Wang, R.; Yu, L. Aggregation Behaviors of Dodecyl Sulfate-Based Anionic Surface Active Ionic Liquids in Water. *J. Phys. Chem. B* **2012**, *116*, 958−965.
(11) Zhao, D.; Fei, Z.; Geldbach, T. J.; Scopelliti, R.; Dyson, P. J. Nitrile-Functionalized Pyridinium Ionic Liquids: Synthesis, Characterization, and Their Application in Carbon - Carbon Coupling Reactions. *J. Am. Chem. Soc* **2004**, *126*, 15876−15882.
(12) Wang, X.; Yu, L.; Jiao, J.; Zhang, H.; Wang, R.; Chen, H. Aggregation Behavior of COOH-Functionalized Imidazolium-Based Surface Active Ionic Liquids in Aqueous Solution. *J. Mol. Liq.* **2012**, *173*, 103−107.
(13) Morrissey, S.; Pegot, B.; Coleman, D.; Garcia, M. T.; Ferguson, D.; Quilty, B.; Gathergood, N. Biodegradable, Non-Bactericidal Oxygen-Functionalised Imidazolium Esters: A Step towards "greener" Ionic Liquids. *Green Chem.* **2009**, *11*, 475−483.
(14) Shukla, S. K.; Pandey, S.; Pandey, S. Applications of Ionic Liquids in Biphasic Separation: Aqueous Biphasic Systems and Liquid−Liquid Equilibria. *J. Chromatogr. A* **2018**, *1559*, 44−61.
(15) Raziq, F.; Humayun, M.; Ali, A.; Wang, T.; Khan, A.; Fu, Q.; Luo, W.; Zeng, H.; Zheng, Z.; Khan, B.; Shen, H.; Zu, X.; Li, S.; Qiao, L. Synthesis of S-Doped Porous g-C3N4 by Using Ionic Liquids and Subsequently Coupled with Au-TiO2 for Exceptional Cocatalyst-Free Visible-Light Catalytic Activities. *Appl. Catal., B* **2018**, *237*, 1082−1090.
(16) Tawfik, S. M. Simple One Step Synthesis of Gemini Cationic Surfactant-Based Ionic Liquids: Physicochemical, Surface Properties and Biological Activity. *J. Mol. Liq.* **2015**, *209*, 320−326.
(17) Postleb, F.; Stefanik, D.; Seifert, H.; Giernoth, R. BIOnic Liquids: Imidazolium-Based Ionic Liquids with Antimicrobial Activity. *Z. Naturforsch., B* **2013**, *68*, 1123−1128.
(18) Gathergood, N.; Garcia, M. T.; Scammells, P. J. Biodegradable Ionic Liquids: Part I. Concept, Preliminary Targets and Evaluation. *Green Chem.* **2004**, *6*, 166−175.
(19) Garcia, M. T.; Ribosa, I.; Gonzalez, J. J.; Comelles, F. Catanionic Mixtures of Surface-Active Ionic Liquids and N-Lauroyl Sarcosinate: Surface Adsorption, Aggregation Behavior and Microbial Toxicity. *J. Mol. Liq.* **2020**, *318*, No. 114040.
(20) Silva, A. T.; Lobo, L.; Oliveira, I. S.; Gomes, J.; Teixeira, C.; Nogueira, F.; Marques, E. F.; Ferraz, R.; Gomes, P. Building on Surface-Active Ionic Liquids for the Rescuing of the Antimalarial Drug Chloroquine. *Int. J. Mol. Sci.* **2020**, *21*, No. 5334.
(21) Feder-Kubis, J.; Wnętrzak, A.; Chachaj-Brekiesz, A. Terpene-Based Ionic Liquids from Natural Renewable Sources As Selective Agents in Antifungal Therapy. *ACS Biomater. Sci. Eng.* **2020**, *6*, 3832−3842.
(22) Mandal, B. Self-Diffusion Studies on Various Miceliee Using Ferrocene as Electrochemical Probe. *Langmuir* **1993**, *0*, 1932−1933.
(23) Lee, J.; Kang, Y.; Kim, J. S.; Park, J.; Lee, J. J.; Kim, B. K. Electrochemical Descaling of Metal Oxides from Stainless Steel Using an Ionic Liquid-Acid Solution. *ACS Omega* **2020**, *5*, 15709−15714.
(24) O'Mahony, A. M.; Silvester, D. S.; Aldous, L.; Hardacre, C.; Compton, R. G. Effect of Water on the Electrochemical Window and Potential Limits of Room-Temperature Ionic Liquids. *J. Chem. Eng. Data* **2008**, *53*, 2884−2891.
(25) McEwen, A. B.; Ngo, H. L.; LeCompte, K.; Goldman, J. L. Electrochemical Properties of Imidazolium Salt Electrolytes for Electrochemical Capacitor Applications. *J. Electrochem. Soc.* **1999**, *146*, 1687−1695.
(26) Mandal, A. B.; Unni Nair, B.; Ramaswamy, D. Determination of the Critical Micelle Concentration of Surfactants and the Partition Coefficient of an Electrochemical Probe by Using Cyclic Voltammetry. *Langmuir* **1988**, *4*, 736−739.
(27) Asakawa, T.; Sunagawa, H.; Miyagishi, S. Diffusion Coefficients of Micelles Composed of Fluorocarbon Surfactants with Cyclic Voltammetry. *Langmuir* **1998**, *14*, 7091−7094.
(28) Docherty, K. M.; Kulpa, C. F. Toxicity and Antimicrobial Activity of Imidazolium and Pyridinium Ionic Liquids. *Green Chem.* **2005**, *7*, 185−189.
(29) Patel, N. N.; Patel, K.; Sastry, N. V.; Patel, V. K.; Macwan, P. M.; Sharma, D. S.; Panjabi, S. H. Halogen-Free COOH Functionalized Surface-Active Ionic Liquids: Surface Activity, Aggregation Behavior, and Antimicrobial Activity. *J. Dispersion Sci. Technol.* **2021**, *0*, 1−11.
(30) Meera, K. M. S.; Sankar, R. M.; Jaisankar, S. N.; Mandal, A. B. Mesoporous and Biocompatible Surface Active Silica Aerogel Synthesis Using Choline Formate Ionic Liquid. *Colloids Surf., B* **2011**, *86*, 292−297.
(31) Jin, Y.; Wang, L.; Wang, T.; Chen, P.; Bi, Y.; Yu, L. Aggregation Behavior of Dodecylsulfonate-Based Surface Active Ionic Liquids in Water. *J. Mol. Liq.* **2015**, *212*, 23−29.
(32) Shaheen, A.; Arif, R.; Waheed, A.; Rehman, S. Synthesis, Physicochemical Characteristics and Antimicrobial Studies of Ethyl-Substituted Imidazolium-Based Surface Active Ionic Liquids (SAILs). *Colloid Interface Sci. Commun.* **2019**, *33*, No. 100204.
(33) Tikariha, D.; Ghosh, K. K.; Barbero, N.; Quagliotto, P.; Ghosh, S. Micellization Properties of Mixed Cationic Gemini and Cationic Monomeric Surfactants in Aqueous-Ethylene Glycol Mixture. *Colloids Surf., A* **2011**, *381*, 61−69.
(34) Sinha, S.; Tikariha, D.; Lakra, J.; Tiwari, A. K.; Saha, S. K.; Ghosh, K. K. Effect of Polar Organic Solvents on Self-Aggregation of Some Cationic Monomeric and Dimeric Surfactants. *J. Surfactants Deterg.* **2015**, *18*, 629−640.
(35) Sastry, N. V.; Vaghela, N. M.; Macwan, P. M.; Soni, S. S.; Aswal, V. K.; Gibaud, A. Aggregation Behavior of Pyridinium Based Ionic Liquids in Water - Surface Tension, 1H NMR Chemical Shifts, SANS and SAXS Measurements. *J. Colloid Interface Sci.* **2012**, *371*, 52−61.
(36) Mandal, M. K.; Barai, M.; Manna, E.; Sultana, H.; Ghosh, R.; Musib, D.; Nag, K.; Kumar Panda, A. Physicochemical Studies on the Interfacial and Aggregation Behavior of Immidazolium- and Pyrrolinidium-Dodecyl Sulfate in Aqueous Medium. *J. Mol. Liq.* **2021**, *337*, No. 116363.
(37) Kumar, H.; Kaur, G. Aggregation Behavior of Mixed Micellar System of Dodecyl Sulfate-Based Surface-Active Ionic Liquids and Anionic Surfactant in Aqueous Media. *J. Surfactants Deterg.* **2021**, *24*, 209−227.
(38) Sun, Y.; Xu, X.; Qin, M.; Pang, N.; Wang, G.; Zhuang, L. Dodecyl Sulfate-Based Anionic Surface-Active Ionic Liquids: Synthesis, Surface Properties, and Interaction with Gelatin. *Colloid Polym. Sci.* **2019**, *297*, 571−586.
(39) Cornellas, A.; Perez, L.; Comelles, F.; Ribosa, I.; Manresa, A.; Garcia, T. T. Self-Aggregation and Antimicrobial Activity of Imidazolium and Pyridinium Based Ionic Liquids in Aqueous Solution. *J. Colloid Interface Sci.* **2011**, *355*, 164−171.
(40) Ghosh, R.; Ekka, D.; Rajbanshi, B.; Yasmin, A.; Roy, M. N. Synthesis,Characterization of 1-Butyl-4-Methylpyridinium Lauryl Sulfate and Its Inclusion Phenomenon with β-Cyclodextrin for Enhanced Applications. *Colloids Surf., A* **2018**, *548*, 206−217.
(41) Vervecken, R. *APPLICATIONS OF IONIC LIQUIDS IN ELECTROCHEMICAL AND CATALYTIC STUDIES Robbe Vervecken* **2015**, 1−8.
(42) Itoh, H.; Ishido, S.; Nomura, M.; Hayakawa, T.; Mitaku, S. Estimation of the Hydrophobicity in Microenvironments by Pyrene Fluorescence Measurements: N-Yβ-Octylglucoside Micelles. *J. Phys. Chem. A* **1996**, *100*, 9047−9053.
(43) Babu, K.; Pal, N.; Saxena, V. K.; Mandal, A. Synthesis and Characterization of a New Polymeric Surfactant for Chemical Enhanced Oil Recovery. *Korean J. Chem. Eng.* **2016**, *33*, 711−719.

https://doi.org/10.1021/acsomega.2c02612
ACS Omega 2022, 7, 28974−28984

(44) Łuczak, J.; Jungnickel, C.; Łącka, I.; Stolte, S.; Hupka, J. Antimicrobial and Surface Activity of 1-Alkyl-3-Methylimidazolium Derivatives. *Green Chem.* **2010**, *12*, 593−601.
(45) Carson, L.; Chau, P. K. W.; Earle, M. J.; Gilea, M. A.; Gilmore, B. F.; Gorman, S. P.; McCann, M. T.; Seddon, K. R. Antibiofilm Activities of 1-Alkyl-3-Methylimidazolium Chloride Ionic Liquids. *Green Chem.* **2009**, *11*, 492−497.
(46) Pernak, J.; Sobaszkiewicz, K.; Mirska, I. Anti-Microbial Activities of Ionic Liquids. *Green Chem.* **2003**, *5*, 52−56.
(47) Qin, M.; Zhong, F.; Sun, Y.; Tan, X.; Hu, K.; Zhang, H.; Kong, M.; Wang, G.; Zhuang, L. Experimental and DFT Studies on Surface Properties of Sulfonate-Based Surface Active Ionic Liquids. *J. Mol. Struct.* **2020**, *1215*, No. 128258.

https://doi.org/10.1021/acsomega.2c02612
ACS Omega 2022, 7, 28974−28984